Composites Science and Technology 237 (2023) 110009

Contents lists available at ScienceDirect

Composites Science and Technology

journal homepage: www.elsevier.com/locate/compscitech

Thermal management in radical induced cationic frontal polymerisation for optimised processing of fibre reinforced polymers

Jeroen Staal [a], Edgar Smit [a], Baris Caglar [b], Véronique Michaud [a,*]

[a] Laboratory for Processing of Advanced Composites (LPAC), Institute of Materials, Ecole Polytechnique Fédérale de Lausanne (EPFL), Station 12, Lausanne, CH, 1015, Switzerland

[b] Aerospace Structures and Materials Department, Faculty of Aerospace Engineering, Delft University of Technology, Kluyverweg 1, Delft, 2629, HS, the Netherlands

ARTICLE INFO

Keywords:
Frontal polymerisation
Polymer-matrix composites (PMCs)
Fiber reinforced polymers
Out-of-autoclave processing

ABSTRACT

Radical induced cationic frontal polymerisation (RICFP) is considered a promising low energy method for processing of fibre reinforced polymers (FRPs). Optimisation of the local heat balance between reinforcement, epoxy resin and the surrounding mould is required to pave the way for its adaptation to an industrial processing method for high volume fraction structural fibre reinforced composites. In this work, we investigate several methods to control the governing heat balance in RICFP-processing of FRPs. Heat generation was controlled by tuning the initiator concentration while limitation of heat losses using highly insulating moulds was found beneficial to the front characteristics and resulting curing degrees. An optimised mould configuration allowed for self-sustaining RICFP in FRPs with fibre volume fractions (V_fs) up to 45.8%, exceeding previously reported maxima of similar systems. A process window was moreover established relating the V_f and required heat generation to the potential formation of a self-sustaining or supported front.

1. Introduction

With the increasing incentive towards more sustainable processing of fibre reinforced polymer (FRP) composites, frontal polymerisation has emerged as a promising out-of-autoclave method that delivers large reductions in environmental impact and processing time compared to traditional (thermal) consolidation methods [1]. Governed by the exothermic heat of polymerisation, frontal polymerisation is characterised by the formation of a distinct separation, i.e. front, between the hot, formed polymer and the cold monomer resin after the application of an initial localised trigger, e.g. thermal or UV-irradiation. The thus-enabled autocatalytic reaction mechanism can then induce autonomous propagation in a front-like manner [2] through the resin, polymerising the FRP in a fraction of the time required by traditional thermal consolidation methods [1,3]. Control of the front temperature is key to the frontal polymerisation process as it governs the front characteristics, such as front velocity as well as the degree of conversion and/or potential degradation of the resin, while fronts are known to quench when insufficient heat is available to overcome the activation energy of the autocatalytic mechanism [2,4]. Assuming an FRP with constant thickness and fibre volume fraction (V_f), the front typically approaches a steady-state temperature which can be directly related to the local heat balance. As schematically illustrated in Fig. 1, the local heat balance of a propagating polymerisation front consists of the exothermic polymerisation enthalpy, thermal diffusion to the neighbouring resin layer thus propagating the polymerisation front, heat losses to the mould and heat uptake by the fibrous reinforcement. The latter term becomes significant in the presence of high V_fs where less heat is generated due to lower resin volumes while more heat is absorbed by higher amounts of fibres, frequently lowering the heat balance below the threshold activation energy required to maintain the front. This currently limits the application of frontal polymerisation to cases where high V_f FRPs are to be produced.

Frontal polymerisation is naturally suitable for acrylate systems, possessing high reactivities combined with relatively low exothermicities, as compared to epoxide systems [5]. Checilo and Enikolopyan [6,7] first observed propagating fronts in highly pressurised methyl methacrylate systems in the early 1970s, while later advances, first reported by Mariani et al. [8], have shown promising potential for systems, e.g. poly(dicyclopentadiene) (pDCPD), undergoing frontal ring opening metathesis polymerisation (FROMP) [1,9–11]. Robertson et al. [1] used FROMP to produce different carbon FRP panels with V_fs up to 51% and demonstrated that resulting properties are comparable to those of oven-cured FRPs. Centellas et al. [12] recently followed up on this and

* Corresponding author.
E-mail address: veronique.michaud@epfl.ch (V. Michaud).

https://doi.org/10.1016/j.compscitech.2023.110009
Received 18 January 2023; Received in revised form 20 March 2023; Accepted 22 March 2023
Available online 23 March 2023

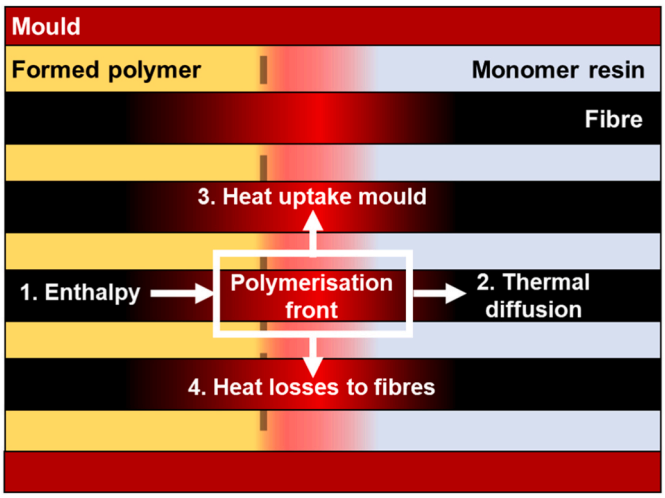

Fig. 1. Schematic representation of local heat balance in frontal polymerisation being composed of 1. Generated enthalpy of polymerisation, 2. Thermal diffusion to boundary layer, 3. Heat uptake by the mould material and 4. Fibrous reinforcements.

showed that similar FRP panels could be produced in a vacuum-assisted resin infusion setup, while multi-point front initiation significantly reduced the processing time. While these studies and other efforts on e.g. recycling [13,14], functionalisation [15–17], additive manufacturing [18–20] and simulation [21,22] clearly demonstrate the potential of FROMP systems, its use in industrial FRP processing is impeded by its relatively short pot life of a few hours, which could be slightly extended in the presence of dedicated inhibitors [23].

With epoxide systems already widely used in the FRP industry, Mariani et al. [24] were the first to propose so-called radical induced cationic frontal polymerisation (RICFP) to induce frontal polymerisation in epoxide resins. Based on radical induced cationic polymerisation proposed by Crivello [25], the autocatalytic mechanism in RICFP is driven by thermal initiation of a free-radical thermal initiator that can accelerate the formation of new activation polymer chains. The dual-initiator configuration of RICFP systems allows for unique resin stabilities, e.g. of over a month while being kept at 50 °C in a dark environment [26], while fronts can be initiated both thermally and by UV-irradiation. While the first studies mainly assessed the compatibility of RICFP systems with different fibre types [27–29], later developments have shown the potential of RICFP as a technique to produce FRPs. Using a system consisting of bisphenol A diglycidyl ether (BADGE), the highly reactive diaryliodonium tetrakis (perfluoro-tert-butoxy) aluminate [30] and benzopinacol [31] as monomer, photoinitiator and thermal initiator, respectively, Dung Tran et al. [3] were able to produce woven carbon FRPs with V_fs of about 35% and mechanical properties comparable to anhydride-cured FRPs. Gachet et al. [32] used novel sulfonium-based initiators and a 3,4-epoxycyclohexylmethyl-3′, 4′-epoxycyclohexane carboxylate (ECC) resin and were able to induce fronts in carbon FRPs with V_fs around 40% with exceptionally high front velocities of over 13 cm/min.

Further bridging the gap to allow the RICFP-processing of FRPs with industrially relevant V_fs, i.e. >55%, requires an optimisation of the process and hence the heat balance near the propagating reaction zone without compromising the resulting FRP properties. This latter requirement impedes the variation of the monomer composition and filler types, which are reported to significantly influence respectively the polymerisation enthalpy and heat uptake during front propagation [3,22,33–35]. Variation of the initiator type and concentration on the other hand has been a proven tool to control the heat generation term in neat polymer systems. The development of novel (photo)initiator types [30,32,36,37] is reported to enhance the reactivity of RICFP systems and thereby potentially the heat generation rate. Control of the heat output of the system is moreover reported to be possible via the initiator concentrations [24,38].

An alternative strategy to shift the heat balance, allowing for the presence of higher V_fs, is to reduce the heat losses of the system to the environment, which has been merely investigated. Knaack et al. [39] observed a relation between the boundary heat losses to the surface-to-volume ratio of a neat RICFP resin, defining a minimum thickness that is required to sustain a front, which was also supported numerically by Tiani et al. [40]. Moreover, numerical work on neat resin systems by Goli et al. [41] suggested that the heat losses to the mould material primarily act at the boundary, lowering the front temperature in the thin layers adjacent to the mould. Centellas et al. [12] and Naseri & Yourdkhani [42] showed that the boundary conditions also affect the front characteristics in a pDCPD-carbon FRP system. The exact role of boundary heat losses in FRP processing however remains unclear and no optimised systems have been proposed to-date.

In this work we present an optimised mould configuration for control over the local heat balance during the RICFP-processing of FRPs. Investigations on the heat output and front characteristics as a function of the initiator concentrations, in combination with a comparative study on the influence of the mould type on the front characteristics and chemical properties of the resulting polymer is presented. Using the optimised process design, carbon FRPs with V_fs that exceed the currently reported maxima for RICFP systems were produced. Variation of the heat generation term gave an insight on the role of the local heat balance in RICFP-assisted FRP processing, allowing for the identification of three distinct regions as function of the V_f and the initiator concentration, i.e.: 1. where a self-sustaining front could be formed, 2. where a front could be formed with additional energy input and 3. where no front could be formed. This work could be of use towards further process and mould optimisation for the RICFP-processing of FRPs, making this system closer to an industrial processing method for manufacturing structural composites.

2. Experimental

2.1. Materials

Resins were based on Omnilane OC1005 (IGM Resins, the Netherlands), containing 3,4-epoxycyclohexylmethyl-3′,4′-epoxycyclohexane carboxylate (ECC) monomer, with photo- and thermal initiators p-(octyloxyphenyl)phenyl iodonium hexafluorostibate (IOC-8 SbF_6, ABCR, Germany) and benzopinacol (Acros Organics, Belgium), respectively, added in various quantities. Small amounts of isopropyl thioxanthone (Genocure ITX, Rahn, Switzerland) were moreover added to shift the initiation wavelength spectrum. The chemical structures of the resin constituents are shown in Fig. 2. 2 × 2 twill weave carbon fibre preform with an areal weight of 285 g/m^2, an ends/picks count of 3.5/3.5 cm^{-1} and 6K fibres per yarn was acquired from Suter Kunstoffe (Switzerland). Moulds were produced from either mould steel, silicone elastomer or a Teflon-covered Diab Divinylcell H60 PVC foam core. High-temperature Polyimide HM 25 μm vacuum bags were acquired from Diatex (France). An EXFO Omnicure S2000 Standard UV-light source was used for UV-irradiation.

2.2. Methods

Resins were purified in a vacuum chamber for 24 hours followed by dissolution of the photo- and thermal initiating and photosensitising compounds under high shear rate. Solutions were degassed under vacuum at room temperature for about 30 min prior to their experimental use.

2.2.1. Heat generation measurement

Investigations on the heat generation term of the local heat balance

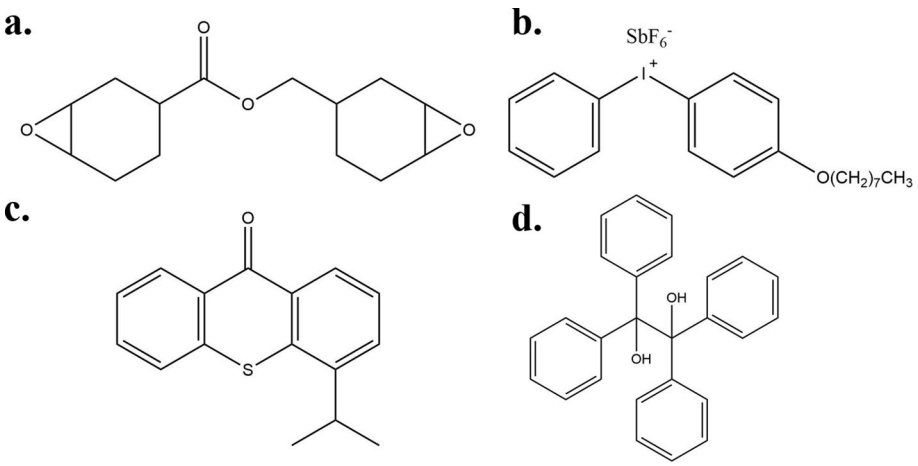

Fig. 2. Chemical structures of the resin constituents: a) 3,4-epoxycyclohexylmethyl-3′,4′-epoxycyclohexane carboxylate (ECC), b) p-(octyloxyphenyl)phenyl iodonium hexafluorostibate (IOC-8 SbF_6), c) isopropylthioxanthone and d) benzopinacol.

comprised a variation of the photo- and thermal initiator contents over a range of 0.5–1.5 w% and 0.22–4.25 w%, respectively. The photosensitiser concentration was kept constant at 0.05 w%. The heat output of the resins was determined using differential scanning calorimetry (DSC, TA Instruments DSC Q100). Samples of 2–3 mg freshly mixed resin were weighed in aluminium hermetic pans. Measurement procedures consisted of an initial heating phase from −20 to 105 °C at a rate of 5 °C/min, followed by an isothermal phase of 30 min. Maximum heat outputs correspond to the recorded peak maxima after baseline correction, as illustrated in Fig. 3a.

Front velocities of these resins were characterised in composite systems containing about 12% V_f extracted carbon fibre tows. The low V_f ensured FP to take place in all studied resin mixtures while simultaneously capturing the influence of the highly conductive carbon fibres. Experiments were carried out in an in-house made silicone elastomer mould with a 45 × 12 × 7 mm cavity volume that was subsequently filled with resin and carbon fibre yarns and closed with the second mould half. Fronts were initiated by the insertion of a soldering pin at one extreme of the mould while temperatures were recorded by three integrated K-type thermocouples placed at respectively 20, 30 and 40 mm from the initiation point. A schematic representation of the experimental setup can be found in Fig. 3b. Thermocouples were connected to

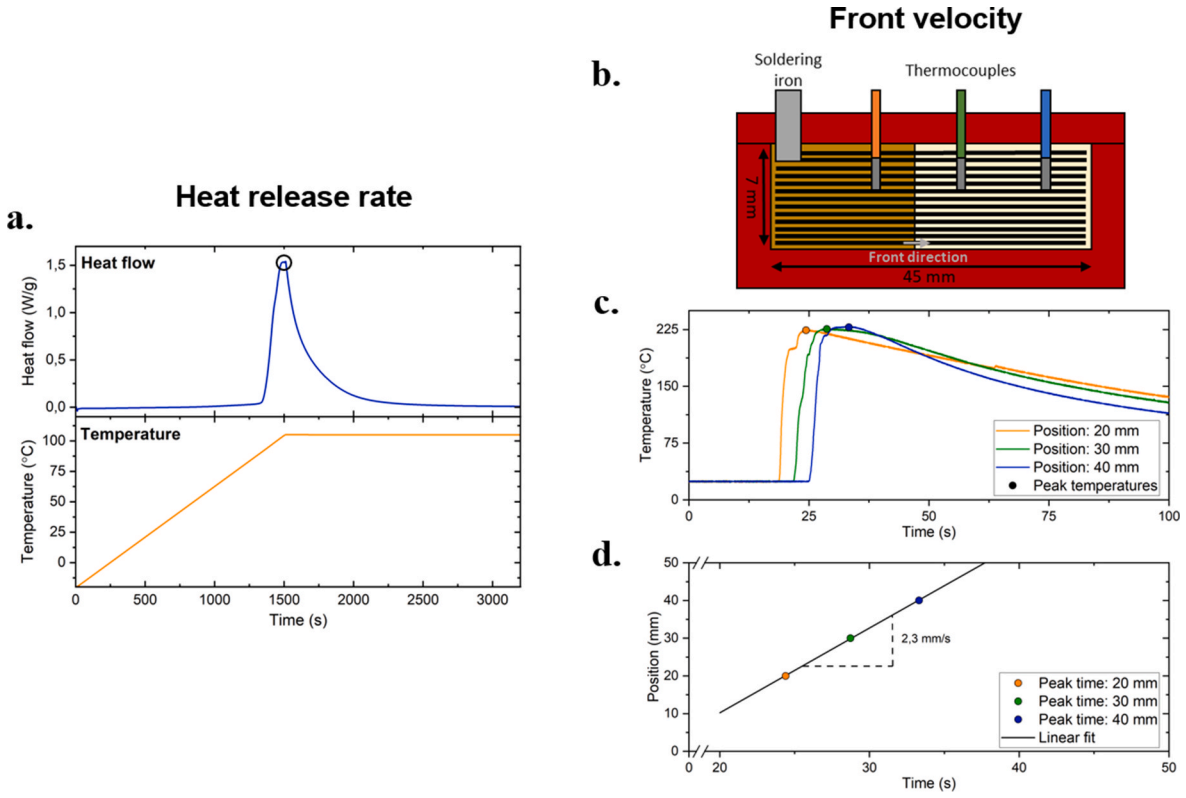

Fig. 3. Overview of experimental procedures for characterisation of the resin exothermicity by a) quasi-isothermal differential scanning calorimetry after baseline correction with the maximum heat output corresponding to the encircled point. b-d) Resulting influence of the heat generation term on front velocities: b) schematic of a longitudinal cut of the mould, indicating the location of the initiation point and thermocouples, c) recorded temperature profiles for a 12% V_f composite system, and d) linear regression of peak instants, corresponding to the maxima of the thermocouple recordings in c), to derive the front velocity.

a National Instruments DAQ device, collecting at an acquisition rate of 100 Hz, coupled to an in-house developed LabView procedure. As demonstrated in Fig. 3c, this allowed for accurate characterisation of the temperature profiles and hence peak temperatures. Front velocities were determined by linear regression of the peak temperatures, illustrated in Fig. 3d. Spearman correlation coefficients of the distributions were determined using the following relation:

$$r = 1 - 6\sum \frac{d^2}{N\left(N^2 - 1\right)} \quad (1)$$

where r is the Spearman's rank correlation coefficient, d the difference in statistical rank of corresponding variables and N the number of variables.

2.2.2. Estimation of the heat losses to the mould

The role of the mould design was investigated on neat resin systems to avoid interference of thermal transport induced by the presence of carbon fibre reinforcements, while initiator concentrations were reduced to avoid degradation of the formed polymer. For these tests, the thermal initiator and photosensitiser concentrations were kept constant at 1 and 0.05% by weight, respectively, while the photoinitiator content was varied between 0.15 and 0.75 w%. An interchangeable mould with a 90 × 35 × 5 mm mould cavity, defined by a silicone elastomer joint and steel spacer, was filled with resin and enclosed by mould halves made of either conductive mould steel, insulating silicone elastomer or Teflon-covered PVC-foam. A schematic representation of the experimental setup and an overview of the thermal properties of the mould materials can be found in Fig. 4a and Table 1, respectively.

Fronts were initiated by UV-irradiation through a 10 mm opening in the upper mould half until front formation was observed. UV-intensities were kept low, i.e. in the order of 125 mW/cm^2, to avoid an initial overshoot of the front temperature. Thermocouples were integrated at 5, 25, 50 and 75 mm from the initiation point and front velocities were derived from the resulting temperature profiles, e.g. Fig. 4b, and linear fitting of the peak times. Interface temperatures between the polymer and mould, under the assumption of perfect thermal contact, were calculated as the weighted mean based on the relative thermal effusivities between the polymer and mould material:

Table 1
Thermal properties of used mould materials.

Material	Thermal conductivity [W/m/K]	Specific heat [kJ/kg/K]	Density [kg/m^3]	Thermal effusivity [kJ/m^2/K/s$^{0.5}$]
Mould steel	32.0[a]	0.46[a]	7850[a]	339.9
Silicone elastomer	0.27[a]	0.50[a]	1450	14.0
Teflon-covered PVC foam core	0.029	1.39[a]	60	1.56
Polymer	0.17	1.20[a]	1165	15.4

[a] Material properties not provided by the supplier are approximated from general material databases.

$$T^* = \frac{e_p T_p + e_m T_m}{e_p e_m} \quad (2)$$

where e_p and e_m the thermal effusivities of the polymer and mould material, respectively, T_p the mean recorded front temperature and T_m the mould temperature away from the interface, taken as 25 °C. Thermal effusivity is given by the square root of the thermal conductivity by the volumetric heat capacity of a given material. Monomer conversion of the formed polymer was assessed by Fourier-transform infrared spectroscopy (FTIR). Strips of about 4 mm were cut transversely to the front direction and subsequently ground to a powder. FTIR signals were recorded over a range of 650–4000 cm^{-1} at a rate of 4 cm^{-1} and spectra were averaged over 64 scans. Conversions were then calculated from the deconvoluted 789 cm^{-1} oxirane absorbance peak height relative to the 1724 cm^{-1} –C═O peak after baseline correction, with uncured resin used as reference material, i.e.:

$$Conversion = 1 - \frac{(A_{786}/A_{1724})_P}{(A_{786}/A_{1724})_R} \quad (3)$$

where A represents the absorbance and subscripts P and R refer to the formed polymer and uncured resin, respectively.

2.2.3. RICFP-assisted FRP processing

Composite production was carried out using a vacuum assisted hand-layup methodology as shown in Fig. 5, using a Teflon-covered PVC foam

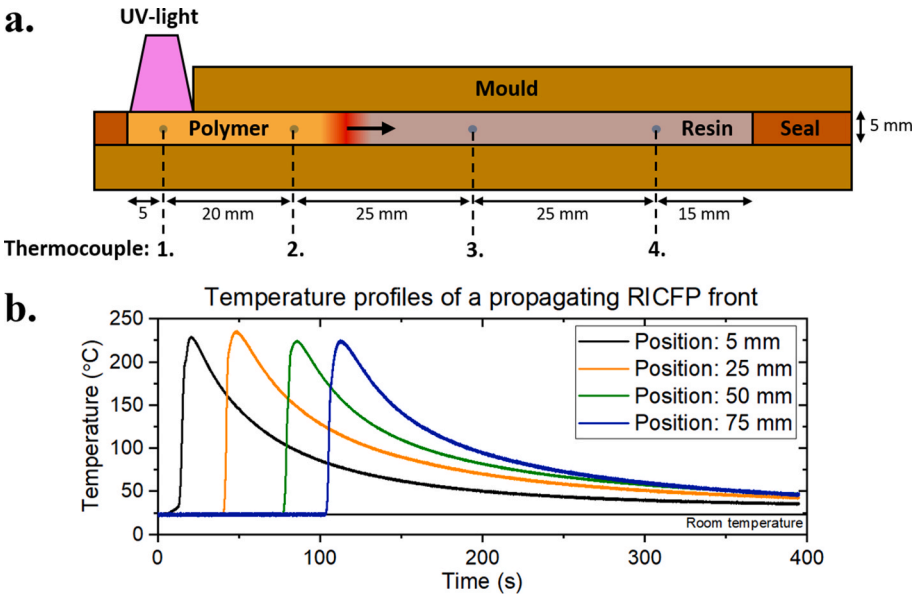

Fig. 4. a) Schematic representation (longitudinal cut) of the mould configuration used for the production of neat polymer and b) exemplary recorded temperature profiles of a propagating RICFP front in a silicon elastomer mould configuration.

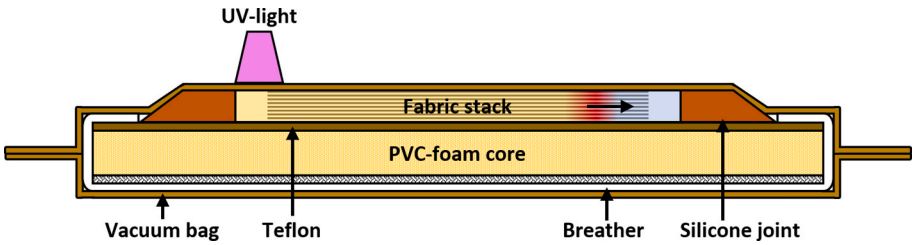

Fig. 5. Schematic representation of experimental configuration for vacuum-assisted hand layup for RICFP-processing of FRPs.

core bottom plate. A vacuum bag was chosen over a foam core top plate to benefit from the increased insulating properties of an air interface. Photo- and thermal initiator contents were varied while keeping a ratio by weight of about 3:4 to limit the degrees of freedom in the assessment while the photoinitiator concentration was generally kept low, i.e. < 1%, as was the case in Section 3.2.2. Resin impregnated 8 × 6 cm carbon fibre preform layers were alternately placed in a 5 mm cavity defined by a silicon elastomer joint, followed by manual compaction of the fabric stack. The completed layup was subsequently enveloped with a high-temperature vacuum bag and the internal pressure was regulated to 500 mbar for a period of 30 min or until a uniform thickness was reached. Front initiation was achieved by high intensity (>500 mW/cm^2) UV-irradiation in one of the resin-rich corners of the mould and the front was left to propagate autonomously. Stalled or quenched fronts were attempted to be re-initiated by UV-irradiation near the front region inside the impregnated fabric stack. The number of fabric layers was varied between 12 and 14 and the final V_f was determined from the final sample thickness, averaged over five different positions, using the following equation:

$$V_f = \frac{nA}{\rho h} \tag{4}$$

where n is the number of fabric layers, A the fabric areal weight, ρ the carbon fibre density, taken as 1.8 g/cm^3, and h the composite sample thickness.

3. Results & discussion

3.1. Heat generation measurement

Optimised RICFP resins for FRP production were expected to mainly benefit from high heat release rates over large polymerisation enthalpies since the influence of concurrent thermal diffusion increases with decreasing heating rates, potentially limiting the front temperatures and complicating activation of the autocatalytic mechanism. Fig. 6a–c shows that increases in photo- and thermal initiator concentrations directly correlated with increased heat outputs, resulting from the increased number of simultaneously growing polymer chains present upon initiation. The increased reactivity of the resin system moreover resulted in increased front velocities, i.e. Fig. 6d–f, which is in line with observations made by Refs. [24,26,38]. Spearman's Rank correlation coefficients listed in Table 2 confirmed that all these recorded trends were significant. Variation of the photosensitiser concentration, shown in Supporting Information 1, did not have any significant influence on both the heat output and the front velocity.

This similarity between these trends moreover confirms the hypothesised relationship between the two parameters, i.e. an increased resin exothermicity can enhance the propagation speed of a travelling front as it allows faster overcoming of the required activation energy for

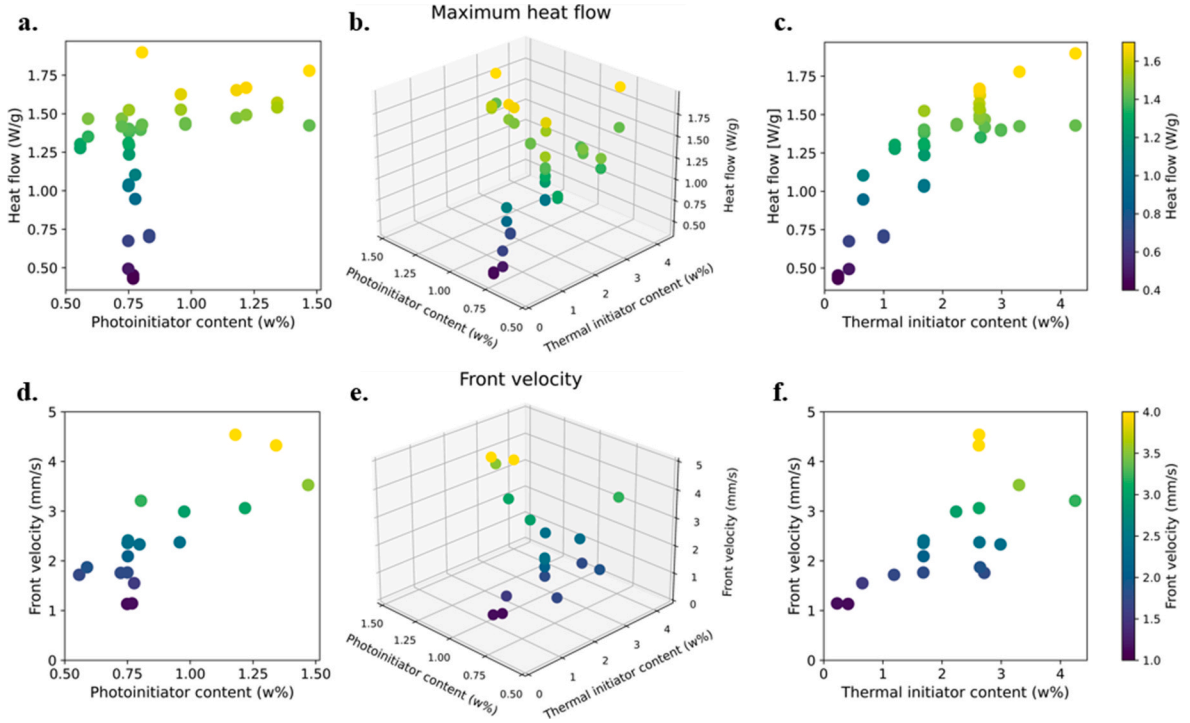

Fig. 6. Heat output of neat RICFP resin recorded in quasi-isothermal DSC measurements with varying concentrations of a) photoinitiator, b) both initiators and c) thermal initiator. Front velocities, recorded by integrated thermocouples, with varying concentrations of d) photoinitiator, e) both initiators and f) thermal initiator.

Table 2
Spearman correlation parameters on the composition dependence of heat outputs and front velocities.

Resin component	Heat output [W/g]		Front velocity [mm/s]	
	Coeff.	$p < 0.05$	Coeff.	$p < 0.05$
Photoinitiator	0.529	$4.6 \bullet 10^{-4}$	0.643	0.018
Thermal initiator	0.759	$1.4 \bullet 10^{-8}$	0.846	$2.7 \bullet 10^{-4}$

localised activation of the autocatalytic reaction mechanism. The thermal initiator concentration appeared to have the largest influence on the maximum heat output, as is supported by the Spearman's Rank correlation coefficients listed in Table 2, showing a strong initial increase and subsequently levelled off above 3 w%. The front velocity in Fig. 6d–f however showed more linear trends as a function of the initiator concentration. The difference in trends between Fig. 6a–c and 6d-f can be largely explained by the thermal degradation and foaming due to excessive heat generation at higher initiator concentrations. This foaming acts as an intrinsic cooling mechanism, lowering the front temperature and hence the front velocity. Since this phenomenon increases with the resin exothermicity, i.e. initiator content, its significance is more visible at the highest concentrations, hence inducing a flattening of the curves in Fig. 6d–f compared to those in Fig. 6a–c. While the onset of thermal degradation at high initiator contents could be avoided by the increased heat losses at higher V_fs, the results in Fig. 6d–f shows the limitation of assessing the role of resin components by the resulting front characteristics. The proposed DSC procedure does not suffer from this behaviour and is therefore considered as the preferred method to characterise the heat output of RICFP resins. The trends observed in Fig. 6 are different from those reported for an ECC resin by Mariani et al. [24]. This difference is believed to result from the use of different initiator types exhibiting different reactivities. The relationship between the heat output of RICFP resins and its initiator concentrations is thus expected to be highly dependent on the resin composition.

3.2. Estimation of heat losses to the mould

Variation of the mould material and thereby the magnitude of heat losses to the environment was found to have only a limited influence on the front characteristics of a neat RICFP system. The recorded front temperatures, shown in Fig. 7a and Table 3, showed a ranking between the conductive steel, insulating silicone elastomer and highly insulating Teflon-covered PVC foam core mould configurations, which was however not significant. The absence of a statistical difference between the mould configurations was attributed to the location of the temperature measurement within the sample, while heat loss effects to the mould are reported [41] to mainly act at the sample boundary. This is confirmed by the calculated interface temperatures in Fig. 7b and Table 3, predicting significant differences of over 80°C between the Teflon-covered PVC foam and silicone elastomer configurations. The predicted interface temperature for metal moulds of ~33–35 °C was insufficient to polymerise the resin close to the interface and a layer of ~0.5 mm typically remained uncured.

The combined results of Fig. 7a & b thus suggest that the choice of mould material and its consequent thermal losses can potentially induce strong thermal gradients over the mould cavity. This prevented the formation of a front at a photoinitiator content of 0.15 w% in a conductive steel mould configuration. Front temperatures at a concentration of 0.75 w% deviated from the apparent linear trends due to the onset of polymer degradation, with foaming of the polymer acting as an intrinsic cooling mechanism. Although this allows for an indication of the maximum front temperatures that could be reached by the current

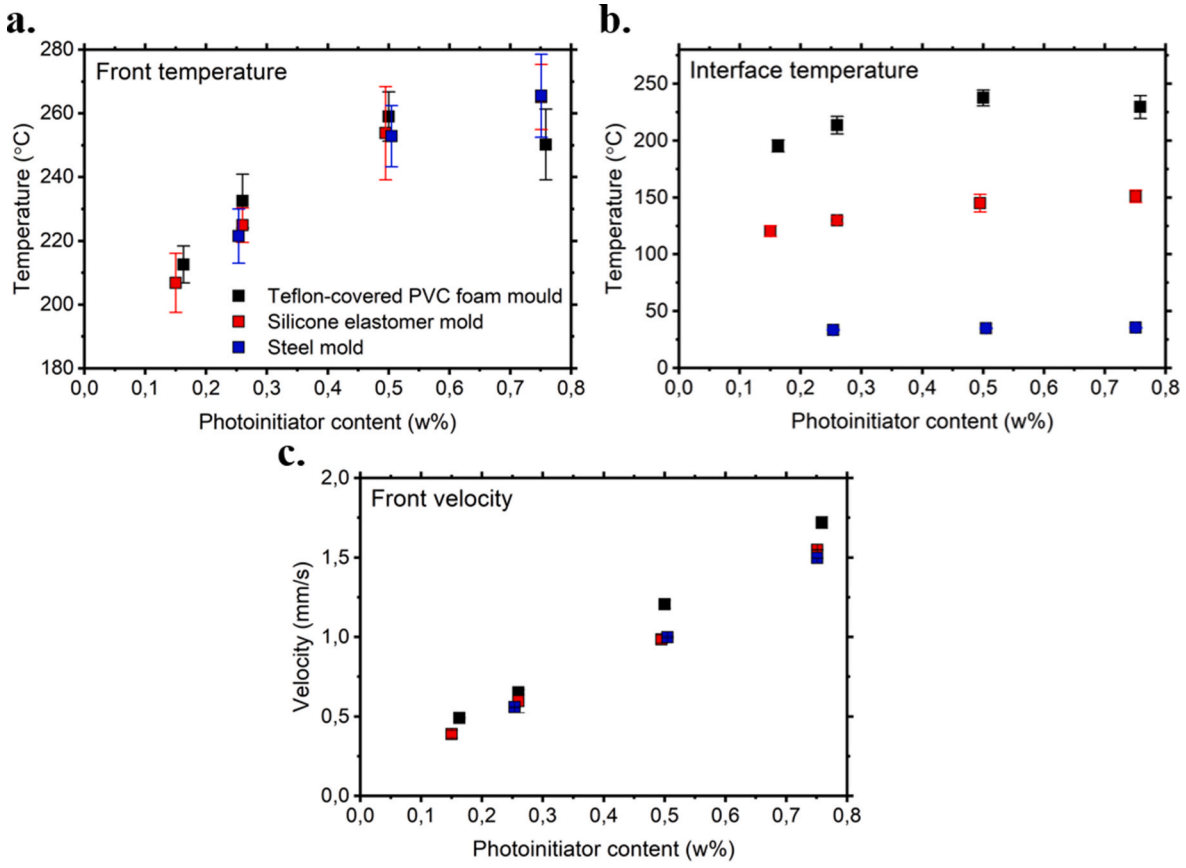

Fig. 7. Comparative overview of front characteristics in neat resin systems with varying resin compositions using different mould types: a) Front temperatures, b) Front velocities, c) Predicted interface temperatures.

Table 3
Comparative overview of front characteristics and resulting monomer conversion of neat polymer samples. Acronym PI denotes the photoinitiator.

PI Content [w%]	Front temp. [°C]	Interface temp.[°C]	Front velocity [mm/s]	Full width at half maximum (FWHM) [s]	Conversion [−]
			Mould steel		
0.15	–	–	–	–	–
0.25	221.5 ± 8.5	33.5 ± 0.4	0.56 ± 0.00	38.9 ± 2.1	0.54 ± 0.08
0.50	252.9 ± 9.6	34.9 ± 0.4	1.00 ± 0.01	35.2 ± 1.4	0.77 ± 0.00
0.75	265.5 ± 13.0	35.4 ± 0.6	1.50 ± 0.00	34.7 ± 2.2	0.96 ± 0.03
			Silicon elastomer		
0.15	206.8 ± 9.3	120.3 ± 4.9	0.39 ± 0.02	113.4 ± 12.3	0.61 ± 0.01
0.25	224.9 ± 5.4	129.8 ± 2.8	0.60 ± 0.07	75.4 ± 7.9	0.67 ± 0.04
0.50	253.8 ± 14.6	144.9 ± 7.6	0.99 ± 0.03	83.4 ± 5.6	0.77 ± 0.01
0.75	265.2 ± 10.2	150.9 ± 5.3	1.55 ± 0.00	81.3 ± 12.8	0.93 ± 0.00
			Teflon-covered PVC foam core		
0.15	212.6 ± 5.8	195.4 ± 5.3	0.49 ± 0.00	470.0 ± 13.1	0.65 ± 0.05
0.25	232.5 ± 8.5	213.5 ± 7.7	0.65 ± 0.01	294.5 ± 15.5	0.68 ± 0.02
0.50	259.0 ± 7.7	237.6 ± 7.0	1.21 ± 0.03	289.7 ± 22.6	0.85 ± 0.02
0.75	250.2 ± 11.1	229.6 ± 10.0	1.72 ± 0.04	172.4 ± 14.9	0.80 ± 0.08

system without degradation of the polymer taking place, the extensive heat uptake by high contents of fibrous reinforcements typically prevents these temperatures to be reached.

The front velocities in Fig. 7c and Table 3 showed similar trends between the conductive steel and insulating silicone elastomer moulds, while they were significantly higher in the Teflon-covered PVC foam core configuration. These trends slightly deviate from those shown in Fig. 7a and give rise to the suggestion that the front velocity depends on the average temperature over (most of) the sample cross-section, i.e. partially capturing the influence of the acting thermal gradients. A relation between the ranking of front velocities in Fig. 7c and the thermal properties of the mould material could moreover be hypothesised. Table 1 shows that the thermal effusivity, representing the ability of a material to exchange thermal energy with its surroundings, of steel is about 20–25 times that of both ECC polymer and silicone elastomer, while the estimated thermal effusivity of a Teflon-covered PVC foam core is about a factor ten lower than that of the latter two materials. The results in Fig. 7c suggest that increased front velocities could be achieved when the thermal effusivity of the mould material is significantly lower than that of the RICFP polymer while front velocities are relatively constant when the thermal effusivity of the mould is comparable or higher.

Assessment of the resulting monomer conversion in Fig. 8a and Table 3 showed a similar general trend where, for photoinitiator concentrations up to 0.5 w%, neat-polymer samples produced in a Teflon-covered PVC foam configuration had higher conversions than those produced in a silicon elastomer mould. Sample conversions of polymer produced in a steel mould configuration were significantly lower at a concentration of 0.25 w% while being comparable to those produced in a silicone elastomer mould at 0.5 w%. It should be noted however that, since only the solid fraction of the sample could be measured (i.e. after removal of the previously discussed uncured sections at the sample top and bottom), the actual conversion over the sample cross-section is expected to be well-below the reported values. The inversed trend between the considered mould configurations at a photoinitiator concentration of 0.75 w% is explained by the severe degradation of the polymer, in particular when produced in the insulating mould configurations, causing interference in the FTIR spectra.

The monomer conversion of RICFP-produced polymer in Fig. 8a ranged on average between 0.6 and 0.85. This is lower than reported for BADGE systems by e.g. Dung Tran et al. [3] and Knaack et al. [39], which is mainly attributed to highly cross-linked network and limited monomer mobility of ECC polymer. Significant improvements are foreseen by the addition of low molecular weight monomers, e.g. 1, 6-hexanediol diglycidyl ether, that possess higher mobilities. The curing degree nevertheless showed larger differences between mould configurations as would initially be expected from the front characteristics, i.e. Fig. 7. While this is partially explained by the strong temperature gradients present over sample cross-section, as concluded from differences in interface temperature shown in Fig. 7b, the mould configuration was also found of significant influence on the cooling phase. As illustrated in Fig. 9, the insulating nature of a silicone elastomer mould and a highly insulating Teflon-covered PVC foam core mould resulted in the polymer samples being subjected to elevated temperatures after passing of the front for a significantly longer period of time as compared to a conductive steel mould configuration. The full width at half maximum (FWHM), i.e. the total time a sample remains above half the peak temperature as illustrated in Fig. 9, in Fig. 8b and Table 3 demonstrate that the cooling stage in a Teflon-covered PVC foam core is significantly longer compared to the other mould configurations. This extended period is believed to act as a post-curing period, increasing the monomer conversion after passing of the front.

3.3. RICFP-assisted FRP processing

The use of a highly insulating Teflon-covered PVC foam core setup was concluded beneficial to the RICFP process and was subsequently used for the production of carbon FRPs. Given a system consisting of a resin with a set initiator concentration and a set carbon fibre V_f, three different scenarios could unfold upon initiation: 1. A self-sustaining

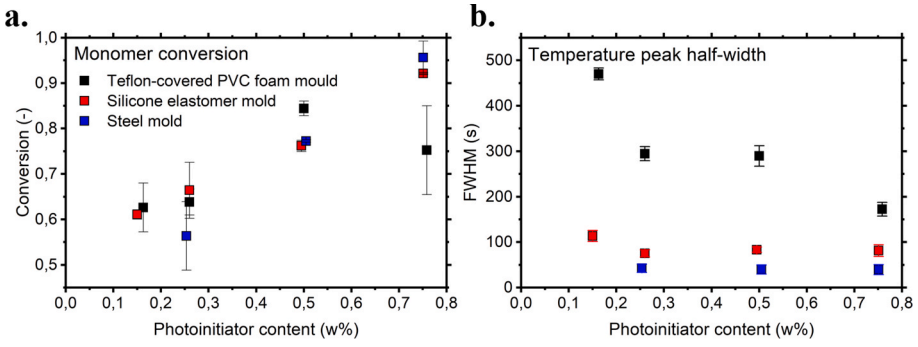

Fig. 8. Resulting distributions of a) curing degree and b) rate of temperature decrease defined by the full-width at half maximum of neat polymer systems with varying initiator contents in different mould configurations.

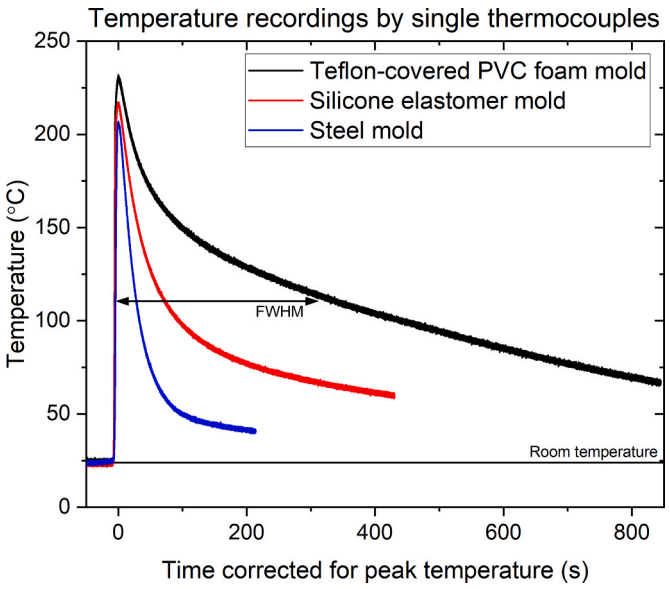

Fig. 9. Demonstrations of temperature profiles recorded by single thermocouples of a RICFP resin containing 0.25% photoinitiator in different mould types.

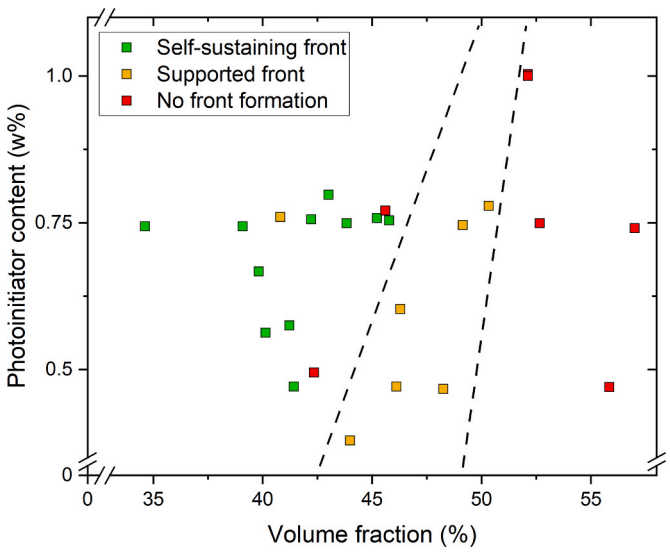

Fig. 10. Relationship between the possibility to form a self-sustaining or supported front as a function of the fibre volume fraction and photoinitiator content in a PVC foam mould. Photo-to thermal initiator ratios generally equalled 3:4 by weight.

front formed and propagated through the fabric stack, 2. The front had to be supported by UV-irradiation or 3. No front could be formed. Fig. 10 shows that these scenarios took place in distinct zones and hence could be used as a process window. A few outliers can be detected in Fig. 10, which are likely a result of difficulties in the thickness control in the vacuum-assisted hand layup setup, inducing local variations in V_f that potentially result in locally increased heat losses and quenching of the propagating front. Further optimisation of the experimental methodology is expected to overcome this. Using the improved mould design in combination with a tuned resin composition, it was possible to induce self-sustaining fronts with V_fs up to 45.8%, exceeding previously published maxima for systems cured by RICFP [3,32]. Supported fronts could moreover successfully cure FRPs with V_fs up to ~50%.

The importance of controlling the local heat balance can moreover be understood from the defined process window. For example, a horizontal movement, where the V_f increases with a constant initiator content, would be expected to gradually reduce the available activation energy for enabling of the autocatalytic mechanism until it falls below its threshold [2,4], which inhibits autonomous front propagation. Introduction of extra energy by means of UV-irradiation would induce an upward shift in the local heat balance and hence overcome the activation energy threshold, allowing for the presence of slightly higher V_fs until it falls below the threshold again. This latter V_f defines the maximum V_f that could be achieved with a certain experimental configuration. The limiting V_fs for the formation of self-sustaining and supported fronts could moreover be adapted with the initiator content, e.g. an increased initiator concentration and hence heat release rate could compensate the heat losses as a result of increased V_fs. While the process will be dependent on the combination of specific resin systems and experimental configurations, its definition could be further employed to optimise RICFP-processing of FRPs, contributing to the application of frontal polymerisation to an industrial composite processing technique.

4. Conclusion

RICFP is regarded as a promising strategy to improve the sustainability and efficiency of epoxide FRP processing. Efforts to-date are limited by the heat uptake of fibre contents, impeding the production of FRPs with V_fs typically encountered in industry. This work aimed at overcoming this limitation by extensive control of the local heat balance, without affecting the resulting FRP properties. Variation of the initiator concentration was confirmed as an effective strategy to control the heat generation term while variation of both the photo- and thermal initiator content played a significant role. The reduced heat losses due to the use of highly insulating mould constituents was found to enhance the front characteristics in a neat-polymer system, which could be translated in an upward shift of the heat balance in FRP systems. Using the improved mould configuration and a tuned resin composition, it was possible to produce FRPs with V_fs of 45.8%, exceeding previously reported maxima for RICFP systems, and reaching meaningful values of fibre content for structural composites, although still with a margin for improvement. A process window was moreover defined that related the possibility to form a self-sustaining or supported front in the proposed experimental procedure as a function of the V_f and initiator content. Future work comprises the further optimisation and development of processing strategies that is expected to contribute to the transformation of RICFP-processing as an established method for FRP manufacturing.

Credit author statement

Jeroen Staal: Investigation, Methodology, Validation, Writing - Original Draft. Edgar Smit: Methodology. Baris Caglar: Methodology, Supervision, Writing - Review & Editing. Véronique Michaud: Conceptualization, Funding Acquisition, Project administration, Supervision, Writing - Review & Editing.

Declaration of competing interest

The authors declare that they have no known competing financial interests or personal relationships that could have appeared to influence the work reported in this paper.

Data availability

Data will be made available on request.

Acknowledgement

The authors acknowledge the financial support from the Swiss

National Science Foundation (SNF n° 200021_182669).

Appendix A. Supplementary data

Supplementary data to this article can be found online at https://doi.org/10.1016/j.compscitech.2023.110009.

References

[1] I.D. Robertson, M. Yourdkhani, P.J. Centellas, J.E. Aw, D.G. Ivanoff, E. Goli, E. M. Lloyd, L.M. Dean, N.R. Sottos, P.H. Geubelle, J.S. Moore, S.R. White, Rapid energy-efficient manufacturing of polymers and composites via frontal polymerization, Nature 557 (2018) 223–234.

[2] J.A. Pojman, Frontal Polymerization, Elsevier B.V., 2012, https://doi.org/10.1016/B978-0-444-53349-4.00124-2.

[3] A. Dung Tran, T. Koch, P. Knaack, R. Liska, Radical induced cationic frontal polymerization for preparation of epoxy composites, Composer Part A Appl. Sci. Manuf. 132 (2020), 105855, https://doi.org/10.1016/j.compositesa.2020.105855.

[4] J.A. Pojman, Cure-on-Demand composites by frontal polymerization, Encycl. Mater. Plast. Polym. (2022) 85–100, https://doi.org/10.1016/b978-0-12-820352-1.00201-7.

[5] B.A. Suslick, J. Hemmer, B.R. Groce, K.J. Stawiasz, P.H. Geu, G. Malucelli, A. Mariani, J.S. Moore, J.A. Pojman, N.R. Sot, Frontal polymerizations : from chemical perspectives to macroscopic properties and applications, Chem. Rev. 123 (2023) 3237–3298, https://doi.org/10.1021/acs.chemrev.2c00686.

[6] N.M. Chechilo, N.S. Enikolopyan, Effect of the concentration and nature of the initiatiors on the propagation process in polymerization, Dokl. Phys. Chem. 221 (1975) 391–394.

[7] N.M. Chechilo, E.I. Khvilivitskii, N.S. Enikolopyan, On the phenomenon of polymerization reaction spreading, Dokl. Akad. Nauk SSSR 204 (1972) 1180–1181.

[8] A. Mariani, S. Fiori, Y. Chekanov, J.A. Pojman, Frontal ring-opening metathesis polymerization of dicyclopentadiene [5], Macromolecules 34 (2001) 6539–6541, https://doi.org/10.1021/ma0106999.

[9] L.M. Dean, A. Ravindra, A.X. Guo, M. Yourdkhani, N.R. Sottos, Photothermal initiation of frontal polymerization using carbon nanoparticles, ACS Appl. Polym. Mater. (2020), https://doi.org/10.1021/acsapm.0c00726.

[10] K.J. Stawiasz, J.E. Paul, K.J. Schwarz, N.R. Sottos, J.S. Moore, Photoexcitation of grubbs' second-generation catalyst initiates frontal ring-opening metathesis polymerization, ACS Macro Lett. 9 (2020) 1563–1568, https://doi.org/10.1021/acsmacrolett.0c00486.

[11] D.G. Ivanoff, J. Sung, S.M. Butikofer, J.S. Moore, N.R. Sottos, Cross-linking agents for enhanced performance of thermosets prepared via frontal ring-opening metathesis polymerization, Macromolecules (2020), https://doi.org/10.1021/acs.macromol.0c01530.

[12] P.J. Centellas, M. Yourdkhani, S. Vyas, B. Koohbor, P.H. Geubelle, N.R. Sottos, Rapid multiple-front polymerization of fiber-reinforced polymer composites, Composer Part A Appl. Sci. Manuf. 158 (2022), 106931, https://doi.org/10.1016/j.compositesa.2022.106931.

[13] E.M. Lloyd, J.C. Cooper, P. Shieh, D.G. Ivanoff, N.A. Parikh, E.B. Mejia, K.E. L. Husted, L.C. Costa, N.R. Sottos, J.A. Johnson, J.S. Moore, Efficient manufacture, deconstruction, and upcycling of high-performance thermosets and composites, ACS Appl. Eng. Mater. 1 (2023) 477–485, https://doi.org/10.1021/acsaenm.2c00115.

[14] O. Davydovich, J.E. Paul, J.D. Feist, J.E. Aw, F.J. Balta Bonner, J.J. Lessard, S. Tawfick, Y. Xia, N.R. Sottos, J.S. Moore, Frontal polymerization of dihydrofuran comonomer facilitates thermoset deconstruction, Chem. Mater. (2022), https://doi.org/10.1021/acs.chemmater.2c02045.

[15] M. Garg, J.E. Aw, X. Zhang, P.J. Centellas, L.M. Dean, E.M. Lloyd, I.D. Robertson, Y. Liu, M. Yourdkhani, J.S. Moore, P.H. Geubelle, N.R. Sottos, Rapid synchronized fabrication of vascularized thermosets and composites, Nat. Commun. 12 (2021) 1–9, https://doi.org/10.1038/s41467-021-23054-7.

[16] Y. Gao, M.A. Dearborn, J. Hemmer, Z. Wang, A.P. Esser-Kahn, P.H. Geubelle, Controllable frontal polymerization and spontaneous patterning enabled by phase-changing particles, Small 17 (2021) 1–9, https://doi.org/10.1002/smll.202102217.

[17] P. Centellas, M. Garg, Z. Chen, X. Zhang, N. Parikh, P. Geubelle, N. Sottos, Energy-efficient manufacturing of multifunctional vascularized composites, J. Compos. Mater. 0 (2022) 1–12, https://doi.org/10.1177/00219983221142353.

[18] Y. An, J.H. Jang, J.H. Youk, W.R. Yu, Frontally polymerizable shape memory polymer for 3D printing of free-standing structures, Smart Mater. Struct. 31 (2022), https://doi.org/10.1088/1361-665X/ac41ea.

[19] Z. Zhang, R. Liu, W. Li, Y. Liu, Z. Pei, J. Qiu, S. Wang, Frontal polymerization-assisted 3D printing of short carbon fibers/dicyclopentadiene composites, J. Manuf. Process. 71 (2021) 753–762, https://doi.org/10.1016/j.jmapro.2021.10.014.

[20] J.E. Aw, X. Zhang, A.Z. Nelson, L.M. Dean, M. Yourdkhani, R.H. Ewoldt, P. H. Geubelle, N.R. Sottos, Self-regulative direct ink writing of frontally polymerizing thermoset polymers, Adv. Mater. Technol. (2022), 2200230, https://doi.org/10.1002/admt.202200230.

[21] E. Goli, I.D. Robertson, P.H. Geubelle, J.S. Moore, Frontal polymerization of dicyclopentadiene: a numerical study, J. Phys. Chem. B 122 (2018) 4583–4591, https://doi.org/10.1021/acs.jpcb.7b12316.

[22] E. Goli, N.A. Parikh, M. Yourdkhani, N.G. Hibbard, J.S. Moore, N.R. Sottos, P. H. Geubelle, Frontal polymerization of unidirectional carbon-fiber-reinforced composites, Composer Part A Appl. Sci. Manuf. 130 (2020), 105689, https://doi.org/10.1016/j.compositesa.2019.105689.

[23] I.D. Robertson, L.M. Dean, G.E. Rudebusch, N.R. Sottos, S.R. White, S. Moore, Alkyl phosphite inhibitors for frontal ring-opening metathesis polymerization greatly increase pot life, ACS Macro Lett. (2017) 609–612, https://doi.org/10.1021/acsmacrolett.7b00270.

[24] A. Mariani, S. Bidali, S. Fiori, M. Sangermano, G. Malucelli, R. Bongiovanni, A. Priola, UV-ignited frontal polymerization of an epoxy resin, J. Polym. Sci. Part A Polym. Chem. 42 (2004) 2066–2072, https://doi.org/10.1002/pola.20051.

[25] J.V. Crivello, S. Liu, Free radical induced acceleration of cationic photopolymerization, Chem. Mater. 10 (1998) 3724–3731, https://doi.org/10.1021/cm980494n.

[26] D. Bomze, P. Knaack, T. Koch, H. Jin, R. Liska, Radical induced cationic frontal polymerization as a versatile tool for epoxy curing and composite production, J. Polym. Sci. Part A Polym. Chem. 54 (2016) 3751–3759, https://doi.org/10.1002/pola.28274.

[27] M. Sangermano, I. Antonazzo, L. Sisca, M. Carello, Photoinduced cationic frontal polymerization of epoxy–carbon fibre composites, Polym. Int. 68 (2019) 1662–1665, https://doi.org/10.1002/pi.5875.

[28] M. Sangermano, A. D'Anna, C. Marro, N. Klikovits, R. Liska, UV-activated frontal polymerization of glass fibre reinforced epoxy composites, Composer Part B. 143 (2018) 168–171, https://doi.org/10.1016/j.compositesb.2018.02.014.

[29] C. Noè, M. Hakkarainen, S. Malburet, A. Graillot, K. Adekunle, M. Skrifvars, M. Sangermano, Frontal-Photopolymerization of fully biobased epoxy composites, 2100864, Macromol. Mater. Eng. (2022) 1–11, https://doi.org/10.1002/mame.202100864.

[30] N. Klikovits, P. Knaack, D. Bomze, I. Krossing, R. Liska, Novel photoacid generators for cationic photopolymerization, Polym. Chem. 8 (2017) 4414–4421, https://doi.org/10.1039/c7py00855d.

[31] D. Bomze, P. Knaack, R. Liska, Successful radical induced cationic frontal polymerization of epoxy-based monomers by C-C labile compounds, Polym. Chem. 6 (2015) 8161–8167, https://doi.org/10.1039/c5py01451d.

[32] B. Gachet, M. Lecompère, C. Croutxé-Barghorn, D. Burr, G. L'Hostis, X. Allonas, Highly reactive photothermal initiating system based on sulfonium salts for the photoinduced thermal frontal cationic polymerization of epoxides: a way to create carbon-fiber reinforced polymers, RSC Adv. 10 (2020) 41915–41920, https://doi.org/10.1039/d0ra07561b.

[33] E. Goli, I.D. Robertson, H. Agarwal, E.L. Pruitt, J.M. Grolman, P.H. Geubelle, J. S. Moore, Frontal polymerization accelerated by continuous conductive elements, J. Appl. Polym. Sci. 47418 (2018) 1–9, https://doi.org/10.1002/app.47418.

[34] Y. Gao, F. Shaon, A. Kumar, S. Bynum, D. Gary, D. Sharp, J.A. Pojman, P. H. Geubelle, Rapid frontal polymerization achieved with thermally conductive metal strips, Chaos 31 (2021) 21–24, https://doi.org/10.1063/5.0052821.

[35] M.S. Malik, M. Wolfahrt, M. Sangermano, S. Schlögl, Effect of a dicycloaliphatic epoxide on the thermo-mechanical properties of alkyl, aryl epoxide monomers cured via UV-induced cationic frontal polymerization, Macromol. Mater. Eng. (2022), 2100976, https://doi.org/10.1002/mame.202100976, 2100976.

[36] R. Taschner, P. Knaack, R. Liska, Bismuthonium- and pyrylium-based radical induced cationic frontal polymerization of epoxides, J. Polym. Sci. (2021) 1–14, https://doi.org/10.1002/pol.20210196.

[37] R. Taschner, R. Liska, P. Knaack, Evaluation of suitable onium tetrafluoroborates for cationic polymerization of epoxides, Polym. Int. (2021), https://doi.org/10.1002/pi.6330.

[38] B.R. Groce, D.P. Gary, J.K. Cantrell, J.A. Pojman, Front velocity dependence on vinyl ether and initiator concentration in radical-induced cationic frontal polymerization of epoxies, J. Polym. Sci. (2021) 1–8, https://doi.org/10.1002/pol.20210183.

[39] P. Knaack, N. Klikovits, A.D. Tran, D. Bomze, R. Liska, Radical induced cationic frontal polymerization in thin layers, J. Polym. Sci. Part A Polym. Chem. 57 (2019) 1155–1159, https://doi.org/10.1002/pola.29375.

[40] R. Tiani, J.A. Pojman, L. Rongy, Critical role of layer thickness in frontal polymerization, J. Phys. Chem. B (2022), https://doi.org/10.1021/acs.jpcb.2c01252.

[41] E. Goli, T. Gai, P.H. Geubelle, Impact of boundary heat losses on frontal polymerization, J. Phys. Chem. B 124 (2020) 6404–6411, https://doi.org/10.1021/acs.jpcb.0c03107.

[42] I. Naseri, M. Yourdkhani, Rapid and energy-efficient frontal curing of multifunctional composites using integrated nanostructured heaters, ACS Appl. Mater. Interfaces 14 (2022) 50215–50224, https://doi.org/10.1021/acsami.2c15415.